Finite Element Modelling of Semi-Rigid Composite Joint in a Slim Floor Frame

Jinming Zeng[1] & Pentti Mäkeläinen[1]
[1]*Department of Structural Engineering and Building Technology, Helsinki University of Technology, FI-02015,TKK, Finland*

jmzeng@cc.hut.fi, pentti.makelainen@tkk.fi

ABSTRACT: In this paper, a semi-rigid composite internal joint in a slim floor frame was modelled by using the general purpose software ABAQUS, a three dimensional (3-D) finite element model was established to analyze the joint behaviour when it is subjected to static loading. The 3D continuum element and truss element were selected to model the main structural parts and the main longitudinal reinforcing bars respectively, and contact condition between all components was modelled explicitly. Mechanical properties, which were theoretically simulated on the basis of the actual measured strength from the test specimens, were used for nonlinear material characteristics in the analysis. For solving the nonlinear problem both in geometry and material properties, static analysis was used in this study. An experimental program also was carried out to test the shear capacity of the joint. Finally, the numerical results were obtained and compared with test results. A good agreement was found between the finite element calculations and the test results.

1 INSTRUCTIONS

A slim floor beam system is defined as steel beams embedded within the slab depth, unlike the situation with a conventional floor beam frame. This system first appeared in Sweden in 1969. Since then it has been predominately used in the frames of multi-storey buildings, mainly in the Nordic countries, but also nowadays in the UK and other European countries. Finland introduced the slim floor beam system about thirty-five years ago; it has become the main structural frame system because of its many advantages, which include the following:
1) the floor depth and lateral stiffness are reduced because of the action of the concrete slab;
2) it gives an increased resistance capacity in ambient and fire situations;
3) it provides good protection against corrosion in damp situations;
4) it allows the convenient hanging and passage of ducts and services.

In recent years, slim floor frames are a widely used structural system, with WQ-beam floor systems being used especially in structural design. How to connect a WQ-beam to a composite column is quite important topic. Designing a reasonable joint system requires the joints to have some characteristics, for example, being economical, ease of fabrication, an abundantly high bearing capacity, and good ductility. There are some joint types that are used to connect a WQ-beam and a composite column already in Finland. However, for the sake of designing more joint types for connecting a WQ-beam with a composite column, a new semi-rigid joint in a slim floor frame is designed. In this paper, the shear capacity of this joint is studied by using finite element program Abaqus.

2 MODELLING

2.1 *Geometric modelling*

Three-dimensional models were created to simulate the joint. In total there are two types of elements to be adopted.

Some main components, such as structural steel and concrete filled in the column, eight-node, first-order solid continuum element (C3D8I) were selected for the modeling. A solid element with incompatible modes has a better performance for such types of problem, including large plasticity calculations, bending, and contact interaction, though these elements take more time, which is expensive. The longitudinal reinforcing bars were modeled via a two-node, first-order truss element (T3D2).

2.2 *Material properties*

All the structural steel parts, such as the WQ-beam, round steel column, console and tension-bar are modeled as an elastic-plastic material with a strain hardening both in compression and in tension, using von-mises plasticity. The modulus of elasticity, yielding stress, and ultimate stress are shown in Fig.1. As shown in Fig.1, the stress-strain curve for structural steel was assigned a three-linear law, its yielding and ultimate stress and yielding and ultimate strain were referred to EN 1993-1-2. Although, the plastic strain deformation at the end of the yielding plateau ε_{st} is not determined in the code, a number of researchers have endeavoured to establish its value by means of experiments or assumptions. Gil, et.al created a formula to calculate ε_{st} with Eq.(1)[4], the results is 2.2%. As for the reinforcement bar, all the key values were determined on the basis of EN1992-1.

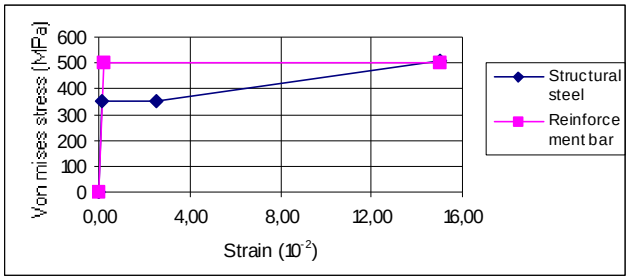

Fig.1 Stress-strain curve of structural steel and reinforcement bar

$$\varepsilon_{.st} = 15 \cdot \varepsilon_{.y} \tag{1}$$

Table.1 Material properties of structural steel and reinforcement bar

Materials	Modulus of elasticity (MPa)	Possion's ratio	Tensile strength f_y (MPa)	Inelastic strain (10^{-2})
Structural steel	210000	0.3	355	0.000
			355	2.370
			510	14.83
Reinforcement bar	200000	0.3	500	15.00

"Damaged plasticity" is used to model the plastic properties of the concrete. This model provides a general capacity for the analysis of concrete structures under static or dynamic and cyclic loading. It is based on the damaged plasticity algorithm. Compared to the companion model (smeared crack model), "damaged plasticity" models concrete behaviour more realistically but at a relatively high cost.

The yield function is based on the Drucker-Prager plasticity model. In this model, the compressive stress-strain curve and tensile stress-strain curve are specified separately. The stress-strain curve

was calculated on the basis of the EN 1992-1. Firstly, the cube strength obtained during the test should be converted into the mean cylinder strength f_{cm} or characteristic cylinder strength f_{ck}. In this study, the mean cylinder strength was adopted. After the f_{cm} has been obtained, on the basis of Table 3.1 shown in EN1992-1, the scant modulus E_{cm}, the strain ε_{c1} at the peak stress can be calculated by using linear regression. The ε_{cu1} at the ultimate states was 0.0035 on basis of Table3-1 in EN1992-1. In Abaqus, the same stress was assumed between the strain ε_{c1} and strain ε_{cu1} in order to make the convergence better. Otherwise, the decreasing curve after the ultimate compressive strain of the concrete was modeled multi-linearly, in which case the non-linearity is smaller and the model converges better. The multi-linear stress-strain relationship also provides a better illustration of the behaviour of the concrete as a bi-linear stress-strain relationship.

The ultimate tensile strength conformed to EN1992-1. The reducing tensile strength of the concrete was simulated with linear stress-displacement, as shown in Fig.3. When the strength reduced faster, the model did not converge. On the other hand, the reducing strength of the concrete has been analyzed. The results were not better, although the strength reduced faster than in this model. In previous studies, the dilatation angle of the concrete varies from 12° to 45°. No significant difference was found in the results obtained with finite element analysis when the dilatation angle of the concrete varied from 20° to 40°. In this model, the dilatation angle adopted was 30°. Considering non-linear material, special for concrete, will make convergence difficult during the finite element analysis. One way to avoid these convergence difficulties is by using the formation of the viscosity μ. In the model, the viscosity of the concrete was specified as very tiny, in which case the model converged better [5]. The material properties of concrete are illustrated in Table2-3 and in Fig.2-3.

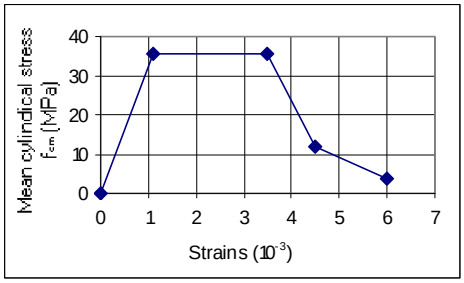

Fig.2 Stress-strain curve of concrete in compression

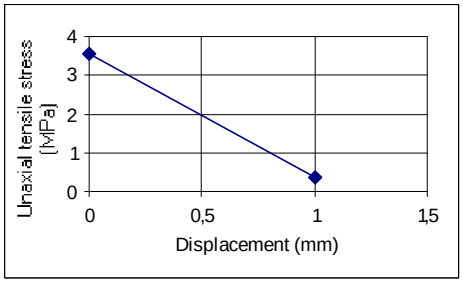

Fig.3 Stress-displacement curve of concrete in tension

Table 2 Material properties of concrete in compression

Material	Modulus of elasticity (MPa)	Possion's ratio	Compressive strength f_{cm} (MPa)	Inelastic strain (10^{-3})
Concrete	31905.7	0.2	35.507	0.000
			35.507	2.387
			11.837	3.387
			3.5507	4.887

Table 3 Material properties of concrete in tension

Material	Tensile stress (MPa)	Displacement (mm)
Concrete	3.551	0.0
	0.3551	1.0

2.3 *Contacts between components*

In the model, all three types of interaction were used to model the contact between components. They are embedded constraints, tie constraints, and friction interaction.

Embedded constraints

The reinforcement is embedded in the solid element (the concrete part of the column), which means that no change is allowed in the spacing and geometry of the reinforcement.

Tie constraints

In this model, all the welded connections between components were modeled by using tie constraints as follows. Surface and surface contact are defined for the tie constraints.

- between the console and the steel part of the column;
- between the tension-bar and the steel part of the column;
- between the tension-bar and the WQ-beam

Friction interactions

Besides the embedded and tie constraints between components, friction interaction is another important method to define the remainder of the contacts. The types of friction interactions are:

- between the tension bar and the concrete part of the column;
- between the steel part of the column and the concrete part of the column;
- between the endplate of the WQ-beam and the console.

Penalty was selected to model the friction formulation and "hard-contact" was considered to simulate normal behaviour. The friction coefficient was 0.3 for the interaction between steel and concrete and 0.2 for the interaction between steel and steel.

2.4 *Boundary condition and loading system*

On the basis of the test set-up, two different boundary condition groups were created: one of them is that a roller support was simulated at the end of the WQ-beam; in this boundary condition only vertical displacement in the z-direction is prevented, and in-plane rotation around x-axis is permitted. The second boundary condition is that the base of the column was clamped to basement.

A uniform pressure load was applied on the top flange of the WQ-beam during the Static General analysis. During the test, in order to exactly simulate the loading situation, the load was gradually applied to the WQ-beam up till failure, as shown in Fig.4. The load site, based on loading site in the test set-up, is 349,95 mm away from the centre of the column. The width of the loading is 20mm.

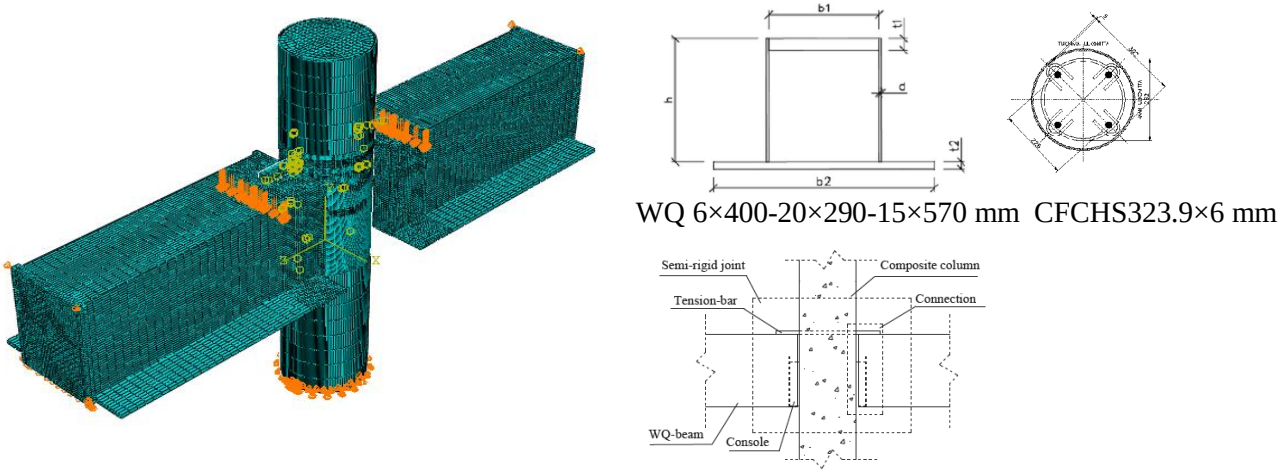

Fig.4 Overview of mesh, boundary condition, loading system, and dimensions of the WQ-beam and the composite column

2.5 *Solution method*

A non-linear analysis was carried out in two steps:

- in the first step, downward displacement of the WQ-beam was applied to the contact surface to make the convergence easier; the downward displacement was only 0.001 mm;
- in the second step, a uniform press force was applied to the top flange of the WQ-beam up till failure as illustrated in Fig.4.

During the analysis, the full Newton method was selected to solve the structure, while automatic control was used to select the increment. It means that the program selects the increments as it de-

velops the response in the step with the objective of obtaining a convergent solution at minimum cost; only the size of the first increment is determined by the user. The minimum and maximum increments were fixed in order to make the analysis as fast and exact as possible.

3 VALIDATION OF FINITE ELEMENT ANALYSIS RESULTS

3.1 *Deformation comparison*

From Fig.5 and Fig.6, similar deformation can be found between the deformation of the specimen in the test results and model results. Specimen failure occurred as a result of something broken appeared on the console, and the endplate of the console was also curled. Plastic deformation appeared on the tension-bar as a result of the major displacement of the WQ-beam.

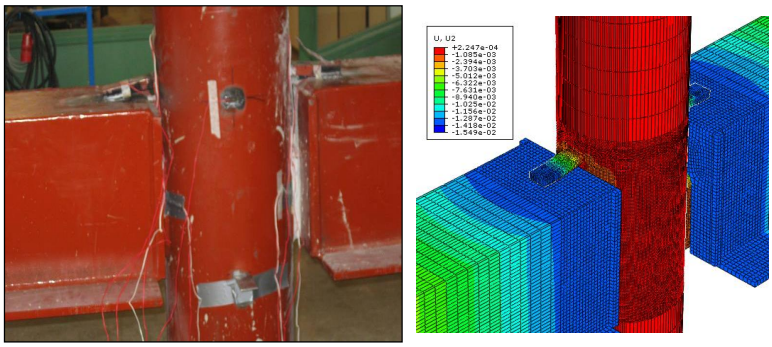

Fig.5 Deformation comparison of the whole specimen

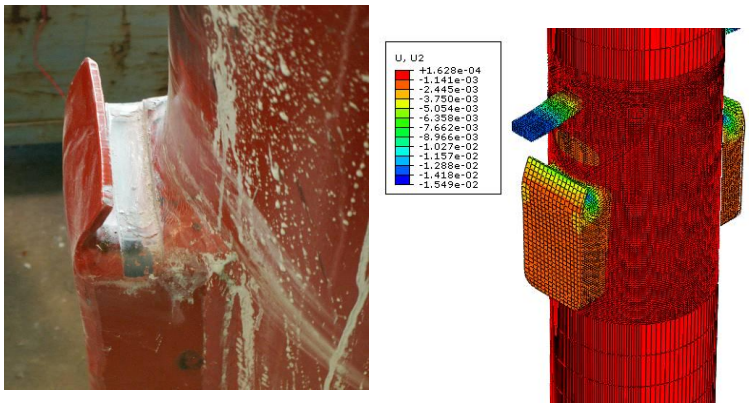

Fig.6 Deformation comparison of the console, the tension-bar, and the column

3.2 *Applied loading-reaction force comparison*

Fig.7 compares the load applied to the WQ-beam and the reaction force in the test model results. Both results show that an almost linear change appeared between the load applied and the reaction force. The model results show good agreement with the test results.

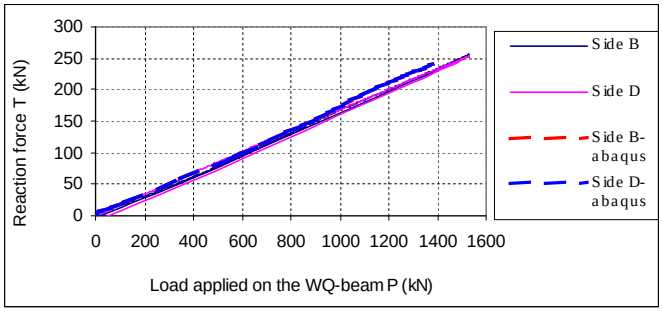

Fig.7 Relationship between load applied to the WQ-beam P and reaction force T

3.3 *Displacement comparison*

Fig.8 compares the WQ-beam displacement S_1-S_4, which were measured through the displacement sensors located underneath the beam webs along the loading lines, between the model results and test results. It can be seen that the model can accurately simulate test results, and a similar change trend in the curve can be found in both results throughout. Fig.9 shows the relative displacement comparison of the console to the column S_5 and S_6, which were measured through the displacement sensors located under the console. The load applied to the joint changed smoothly with the relative displacement as shown in the test results. Both sets of results showed a similar change trend. The curve between the relationship of the column shaft displacement S_7 and S_8, which were measured through the displacement sensors located at the column shaft beneath the support line of the beam, and the load applied to the column (Q) obtained from the test and model analysis is compared in Fig.10. It can be seen that the model results show fair agreement with the test results throughout; they had a similar change trend**.**

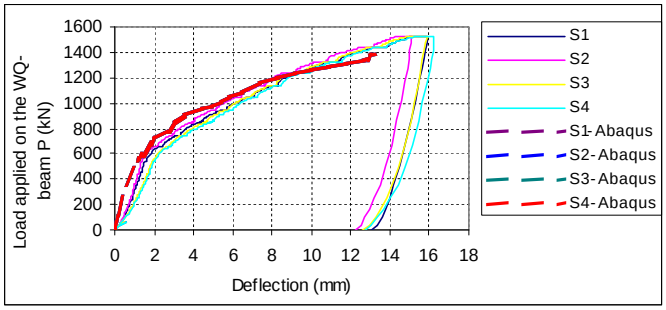

Fig.8 Relationship between load applied to the WQ-beam P and deflection S_1..S_4 of WQ-beam

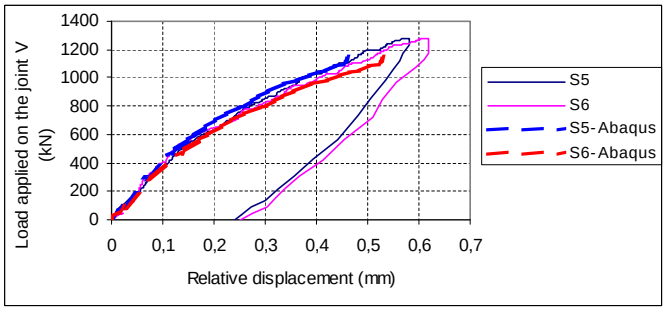

Fig.9 Relationship between load applied to the joint V and relative displacement S_5..S_6 of the console based on the column shaft

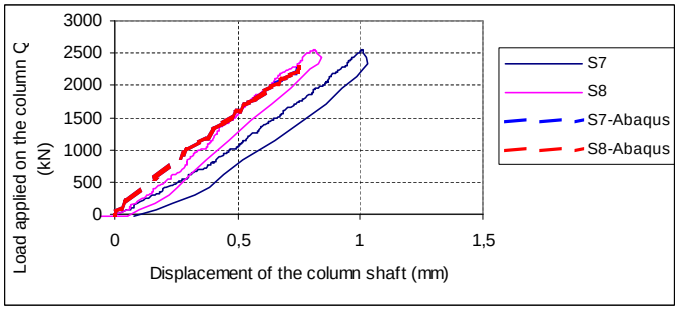

Fig.10 Relationship between load applied to the column Q and displacement of the column shaft in relation to the laboratory floor S_7..S_8

3.4 *Strain comparison*

A comparison of the strain (L_{41} and L_{42}) localized on the column shaft in test results and model results is shown in Fig.11. It can be concluded that the model results show agreement with the test results. A similar change trend can be found in both sets of results. Fig.12 shows comparison between the strain (L_{43} and L_{44}) on the tension-bar in the test and model results. The strain obtained in the model analysis is quite close to the results in the test. The comparisons between the strain (L_{45}-L_{48}) in the column above the tension-bar in the test results and model results are illustrated in

Fig.13-14. It can be seen that they have slight difference, as the model analysis cannot exactly simulate the situation caused by welded failure. Fig.15-16 shows the strain comparison (L_{61}-L_{64}) on the web of the console. A good fit can be found between the model and test results, the strains were accurately simulated in the model.

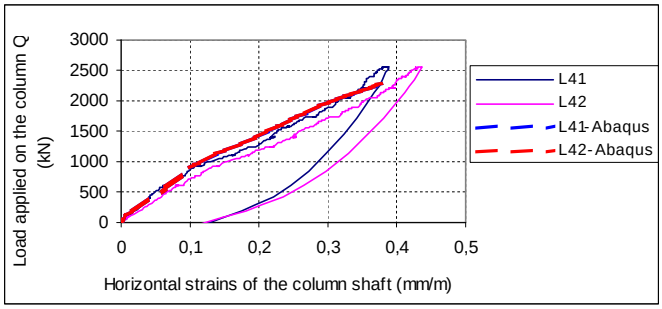

Fig.11 Relationship between load applied to the column and horizontal strains of the column shaft

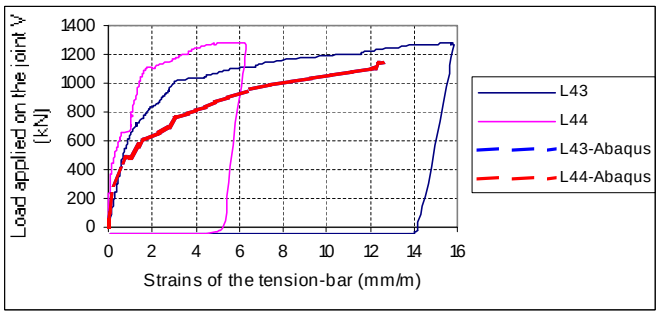

Fig.12 Relationship between load applied to the joint V and strains on the tension-bar

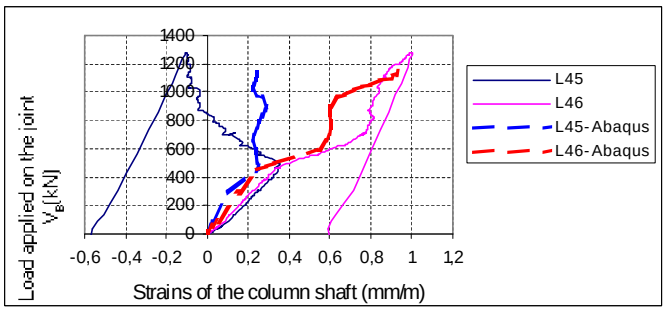

Fig.13 Relationship between load applied to the joint V_B and the strains of the column shaft for B-side

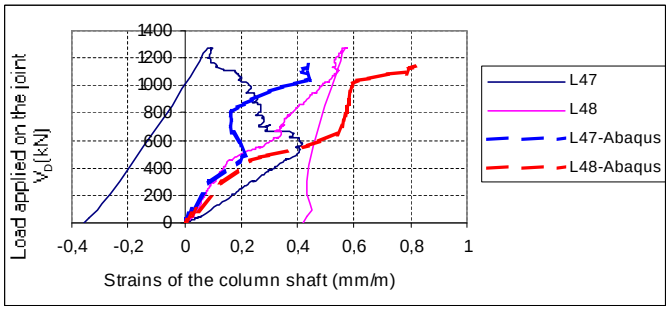

Fig.14 Relationship between load applied to the joint V_D and the strains of the column shaft for D-side

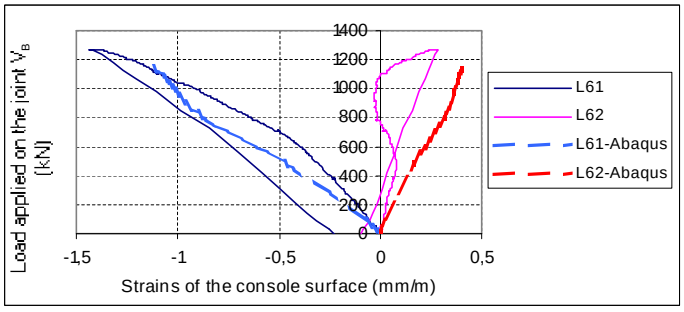

Fig.15 Relationship between load applied to the joint V_B and the strains on the console surface for B-side

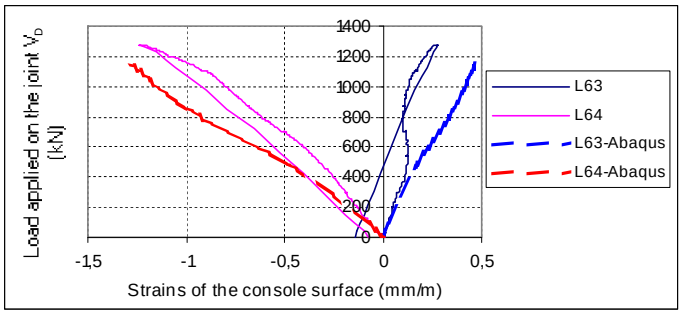

Fig. 16 Relationship between load applied to the joint V_D and the strains on the console surface for D-side

4 CONCLUSIONS

The shear capacity of the joint was investigated by finite element analysis with Abaqus, and which results were compared to the test results. The model results showed the same failure mode in the test; the specimen failed in the console. Good agreement was observed in the deflection, loading, and strain comparisons. The model analysis can exactly simulate the test.

ACKNOWLEDGEMENT

This study is financial supported by the Finnish company, Rautaruukki Oy, which is gratefully acknowledged. The author would like to thank to Mr. Kansa Jouko and Ms. Virta Tarja for their advices to this study.

REFERENCES:

[1] ABAQUS/Standard, User's Manual, version6.7, Hibbitt, Karlsson & Sorensen Inc., 2007
[2] Suomen Standardisoimisliitto SFS. Eurocode 3: Design of steel structures. Part 1-1: General rules and rules for buildings, EN 1993-1-2:2005
[3] Suomen Standardisoimisliitto SFS. Eurocode 2: Design of concrete structures. Part 1-1: General rules and rules for buildings, EN 1992-1-1:2004
[4] Beatriz Gil & Eduardo Bayo. An alternative design for internal and external semi-rigid composite joints. Part II: Finite element modeling and analytical study. Engineering Structures 2008; 30;232-246.
[5] Richard Malm. Shear cracks in concrete structures subjected to in –plane stresses, Stockholm, Sweden, PhD thesis. 2006, Royal Institute of Technology (KTH), Department of Civil and Architectural Engineering, Division of Structural Design and Bridges